A New Dental Superalloy System: III. Microstructure and Phase Transformations

HAMDI MOHAMMED, KAMAL ASGAR, and W. C. Bigelow*
University of Michigan, Ann Arbor, Michigan 48104, USA

A microstructural study was conducted on 15 cobalt-chromium-nickel alloys of the basic composition 40 Co-30 Ni-30 Cr. The alloys were strengthened by the addition of tantalum and tantalum-rich regions were found at the interdendritic spaces. The increase in Ta concentration caused a decrease in the concentration of the β phase and an increase in the amounts of the α phase. Excessive amounts of Ta resulted in formation of the σ phase. The failure of the alloy occurred as a result of the interconnection of σ regions.

In part I of this series of articles, alloy design was discussed. It was stated that the addition of tantalum (Ta) to cobalt (Co)-chromium (Cr)-nickel (Ni) alloys may stabilize the ductile face-centered cubic (FCC) phase and should decrease the concentration of the less ductile hexagonal close-packed (HCP) phase.[1] The experimental results of mechanical testing were presented in part II of this study; they showed that the addition of Ta produced stronger and more ductile Cr-Co alloys.[2] These results indirectly support the aforementioned statement, although a direct observation of the transformation has not been obtained. In part I it was found that Ta reacts with Co to produce the intermetallic compound Co_3Ta, that excessive concentrations of Ta resulted in the formation of the sigma phase, and that the σ phase causes alloy brittleness.

The purpose of this investigation was to conduct metallographic examinations that would reveal the effect of the addition of various concentrations of Ta on the microstructure of the ternary base alloy.

Materials and Methods

A specimen of each of the alloys tested in part II was used for the metallographic examination. Half of the tensile specimen was cut into two pieces. The threaded portion was mounted perpendicularly and the bar portion was mounted horizontally in a polyester resin block. Each block had a cross section and a longitudinal section of the specimen. The specimens then were ground and polished with various grades of Carborundum and levigated alumina. The last alumina grade used was 0.05 micrometers in diameter. Then, automatic polishing was done† for two hours.

Most of the etchants that were used for the Co-base alloys failed to etch the quaternary alloys. Etchants of hydrofluoric acid etched the Ta-rich phase only, but there was severe pitting. A modified perchloric acid etchant that was designated as *E*-1 revealed the Ta-rich phase without pitting. To differentiate the other phases in the alloys, a second etchant that was designated as *E*-2 was used after etching with *E*-1. All specimens were etched electrolytically by both etchants. The composition and method of application of both etchants are given in Table 1. A research metallograph‡ was used to examine and photograph the specimens. The alloys were examined at magnifications of ×250, ×500, ×1,000, and ×2,000 and they were photographed at ×250 and ×1,000 magnifications. A photomicrograph

Based on a dissertation submitted in partial fulfillment of the PhD degree in dental materials and engineering materials at the University of Michigan, 1971.

Received for publication May 14, 1972.

* Present address: University of Connecticut, Health Center, School of Dental Medicine, Farmington, Conn 06032.

† Syntron vibratory parts feeder, type LPO.O, Homer City, Pa.

‡ Model VE, Bausch and Lomb Optical Company, Rochester, NY.

TABLE 1
ETCHANTS USED IN REVEALING THE MICROSTRUCTURE

Etchant	Composition	Application
E_1	12 ml Distilled Water 70 ml Ethanol 70 ml Glycerol 8 ml Perchloric Acid	Electrolytic 25 v 0.8 amps Pt electrode
E_2	20 ml Glycerol 80 ml Hydrochloric Acid 5 ml Nitric Acid 40 ml Distilled Water 1 gm Cupric Chloride	Electrolytic 10 mv 500 ma C electrode

of specimen A_8B_8 (10.2% Ta) that was etched with E-1 is shown in Figure 1. The same specimen that was etched with E-1 and E-2 is shown in Figure 2.

The microhardness of the various phases was determined as a supplement to phase identification and to test for phase transformation. A microhardness tester,* a Knoop indenter,† a 25 gm load, and a 4mm objective lens (×750) were used.

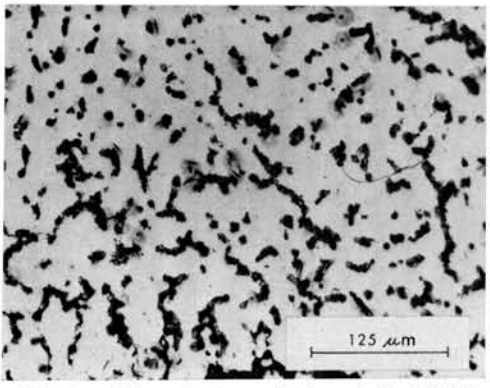

FIG 1.—Microstructure of alloy A_8B_8 (10.7% Ta), etched by E-1 only.

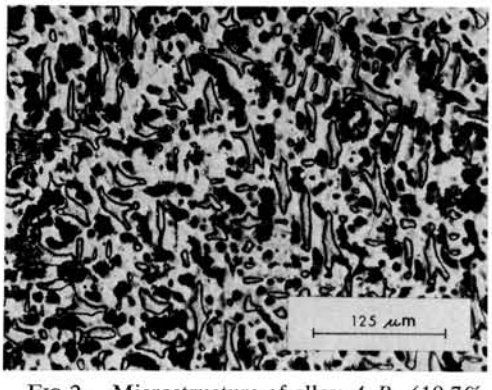

FIG 2.—Microstructure of alloy A_8B_8 (10.7% Ta), etched by E-1 and E-2.

Results

The micrograph of alloy A_1B_1 that contained no Ta (Fig 3), revealed three phases: a continuous matrix phase; a discontinuous phase; and a third phase that appeared as black dots in the matrix region. The matrix is called C, the discontinuous phase is called D, and the third phase that appears in the C region is designated as A.

The addition of 2% (A_2B_2) to the alloy base did not cause a significant change in the microstructure of the alloy. The amount of D phase decreased and then disappeared when the Ta content was increased. The gradual decrease of phase D is illustrated in Figures 3 to 6; these alloys contained 0 to 15.2% Ta. Figures 3 to 6 demonstrate that a new phase was precipitated within the C phase; this phase is called B and its amounts increased with Ta concentration.

In the microstructure of alloys with higher concentrations of Ta (more than 12%), there was a precipitation of larger quantities of phase A. The quantities of A increased with Ta as can be seen in Figures 5 and 6. An equivalent change in Ta concentration in alloys that contained less than 12% Ta does not cause a large change in the amount of phase A.

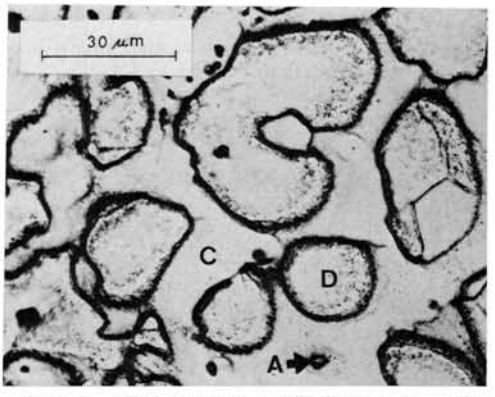

FIG 3.—Microstructure of alloy A_1B_1 (0% Ta). C, matrix; D and A, phases.

* Tukon, Wilson Instrument Division of American Chain & Cable, New York, NY.

† Knoop, Wilson Instrument Division of American Chain & Cable, New York, NY.

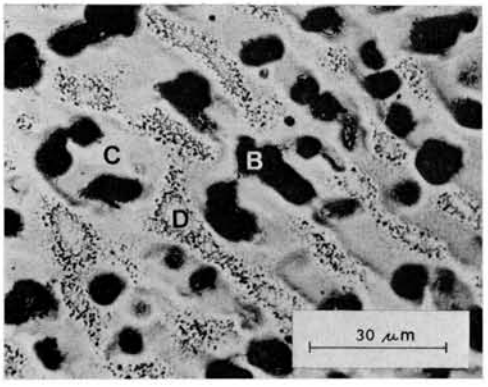

FIG 4.—Microstructure alloy of A_7B_7 (9.1% Ta). *C*, matrix; *D* and *B*, phases.

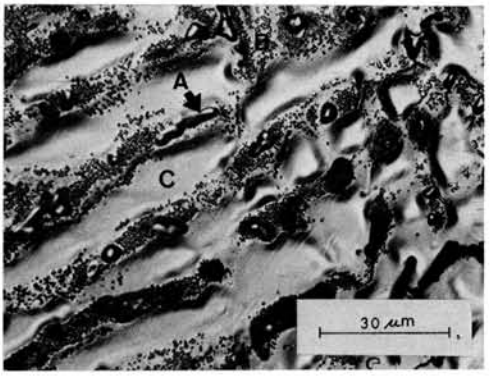

FIG 7.—Microstructure of alloy $A_{13}B_{13}$ (13.8% Ta), light etching. *C*, matrix, *A*, phase.

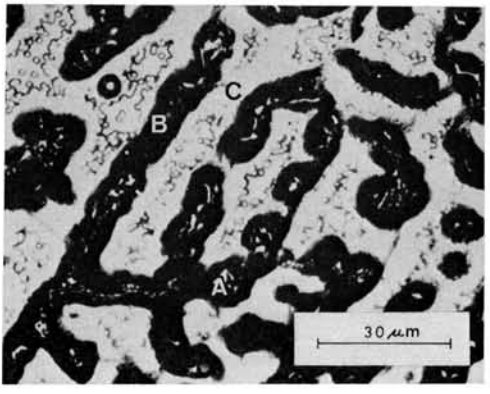

FIG 5.—Microstructure of alloy $A_{11}B_{11}$ (13.0% Ta). *C*, matrix; *B* and *A*, phases.

A light etching of the alloys (Fig 7) reveals that phase *A* has a vitreous appearance that is characteristic of σ-type phases. Phase *B* has small colonies of precipitate.

The relationship between the *A* phase and crack initiation can be studied by comparing Figures 8 to 10. These three figures are one specimen; the only difference is the distance from the fractured end. As the figures indicate, the various regions of *A* are connected by minor fractures.

A summary of the microhardness test results of the various phases is given in Table 2. Table 2 illustrates that the hardness of phase *D* remained constant and that of phase *B* increased slightly with Ta concentration. Phase *A* was the hardest phase in all instances. Phase *C* decreased in hardness with Ta up to 7.4%; then, its hardness increased gradually with Ta. Before the

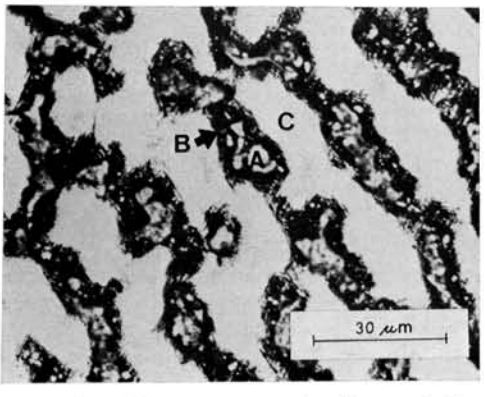

FIG 6.—Microstructure of alloy $A_{14}B_{14}$ (15.2% Ta). *C*, matrix; *B* and *A*, phases.

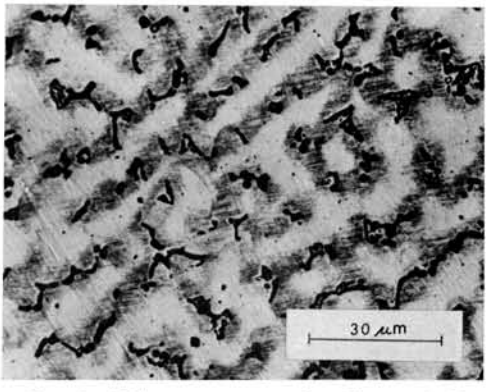

FIG 8.—Microstructure of alloy $A_{15}B_{15}$ (16.7% Ta), away from fractured end.

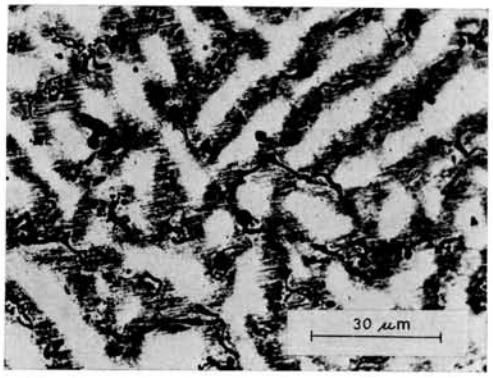

FIG 9.—Microstructure of alloy $A_{15}B_{15}$ (16.7% Ta), 4 mm from fractured end.

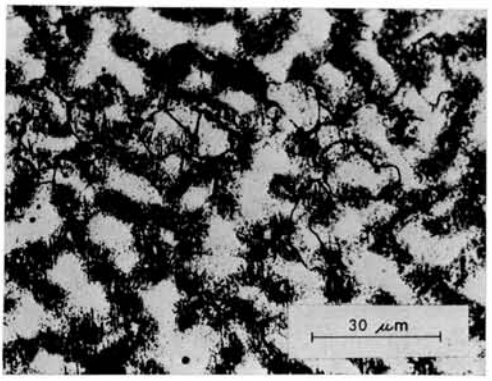

FIG 10.—Microstructure of alloy $A_{15}B_{15}$ (16.7% Ta), 2 mm from fractured end.

behavior of phase *C* could be accepted, a statistical analysis was necessary. An analysis of variance[3,4] (Table 3) demonstrated that the hardness of Phase *C* in the various alloys is different. The values that are different and those that are the same were determined by ranking. In Table 4 the values that are underlined by the same line are equal. For example, the hardness of phase *C* in alloys $A_{13}B_{13}$ and $A_{15}B_{15}$ is the same, whereas that of alloy A_7B_7 is lower than the hardness of phase *C* in alloy A_1B_1. The statistical analysis illustrates that the hardness of phase *C* in the alloys decreased with Ta to a certain concentration; beyond this concentration the phase hardened as Ta concentration was increased.

TABLE 2
SUMMARY OF HARDNESS TESTING RESULTS

Alloy Designation	Ta (%)	Hardness KHN			
		A	*B*	*C*	*D*
A_1B_1	0	514	NP*	460	367
A_3B_3	3.9	523	NP	423	380
A_5B_5	5.7	580	507	395	372
A_6B_6	7.4	585	501	381	374
A_7B_7	9.1	580	506	444	376
A_8B_8	10.7	586	507	500	370
A_9B_9	12.3	612	507	499	377
$A_{11}B_{11}$	13.0	768	552	515	NP
$A_{13}B_{13}$	13.8	751	561	527	NP
$A_{14}B_{14}$	15.2	756	573	529	NP
$A_{15}B_{15}$	16.7	772	570	525	NP

* NP, not present.

Discussion

The aforementioned alloys were made from a basic ternary alloy with the composition of 40 Co-30 Ni-30 Cr. This alloy was chosen from the ternary phase diagram because it conforms to the requirements specified for a Co-base alloy that were discussed in part I of this study.[1] The alloy

TABLE 3
SUMMARY OF ANOVA FOR HARDNESS OF REGION C IN THE PREPARED ALLOYS

Source of Variation	*df*	Sum of Squares	Mean Square	*F* Ratio
Among treatments	11	359,207.9	32,655.3	$F = 144.84$
Within treatments	108	24,249.1	225.2	$F_{0.99}(11,108) = <3$
Total	119	383,557.0		

TABLE 4
RESULTS OF DUNCAN'S NEW MULTIPLE RANGE TEST FOR REGION C IN THE PREPARED ALLOY

A_6B_6	A_5B_5	A_3B_3	A_2B_2	A_7B_7	A_1B_1	A_9B_9	A_8B_8	$A_{11}B_{11}$	$A_{15}B_{15}$	$A_{13}B_{13}$	$A_{14}B_{14}$
381	392	395	423	444	460	498	500	515	525	527	529

Note: Values underlined by the same line are equal.

contains three phases. The concentrations were calculated from the phase diagram to be 72% α, 11.5% β, and 16.5% σ; α is a solid solution of Cr in an FCC matrix of Co and Ni, β is a similar solid solution in an HCP matrix, and σ is a solid solution of Ni in a body-centered tetragonal (BCT) matrix of Co and Cr. Other studies indicate that σ is the hardest phase that forms in the superalloys[5] and that the β phase should be harder than the α phase because of its crystal structure. Slip, which determines ductility, usually takes place first on the crystallographic plane that has the greatest number of atoms. These are the weakest planes because they are separated by the greatest interplanar distances; therefore, they have a low degree of interatomic attraction. The number of planes that is favorably located for slip to occur depends on the particular crystal lattice. The availability of potential slip systems in the cubic lattice may account for the relatively low hardness of the α phase that crystallizes in this system.

When the result of the various testing methods that were used on alloy A_1B_1 are combined, the major and softest phase in the alloy (phase *D*, Fig 1) is α. The next hardest phase (*C*, Fig 1) is β, and the hardest phase (*A*, Fig 1) is σ. This conclusion conflicts with the phase-ratio calculation, which shows that the β phase should be 11.5%. The photomicrograph of Figure 1 indicates that the continuous phase, which is marked *C*, is more than 11.5%. The aforementioned conclusion is also contradicted by the fact that the hardness of the α phase was reported[6] to be KHN 300; this is lower than the value of KHN 367 that was obtained in this study.

On the basis of hardness results, phase *A* in Figure 1 can be accepted as σ, and phase *D* can be accepted as α + β. The nature of phase *C* will be determined later in the discussion.

Phase *B*, which begins to appear when Ta concentration is higher than 6% and increases in concentration with Ta, can be considered Co_3Ta. The latter conclusion is supported by an X-ray diffraction analysis, which will be presented in part IV of this study.

The nature of phase *C* has not yet been identified. The hardness of phase *C* decreased from KHN 460 for the alloy that had no Ta to KHN 381 when Ta concentration was 7.4%. At this concentration of Ta, the hardness of phase *C* and that of phase *D*, which was identified as α + β, are equal.

The addition of Ta results in a decrease of the hardness of phase *C* only if it causes the unstable α → stable α transformation. In part I, the stacking fault energy (SFE) theory was introduced.[1] It was indicated that the addition of Ta raises the SFE and stabilizes the face-centered cubic α phase. A region of unstable α has a high concentration of stacking faults; it is a region of α that has small regions of β within it. These stacking faults harden and embrittle the region as a result of inhibition of the flow of dislocations. The addition of Ta raises the SFE and stabilizes the α phase. Stabilization of the α phase is a process that eliminates stacking faults and softening. Therefore, the continuous *C* phase in Figure 3 may be called unstable α.

This conclusion can be supported by two more arguments. First, the σ phase limits its precipitation to the continuous phase *C*. Sims[5] indicated that stacking faults precede σ formation in σ-prone alloys; the existence of stacking faults or σ is an indication of the presence of the other.

Secondly, Johnson's[6] work supports the aforementioned conclusion. When the hardness of what he called unstable α + β was obtained, transformation striations were observed at the periphery of the indentation. These striations indicate the α → β transformation. Similar striations were obtained in the C region in the alloys that had less than 8% Ta. A photomicrograph of these striations in alloy A_3B_3 (3.9% Ta) is illustrated in Figure 11.

The disappearance of phase *D*, which was defined as α + β, with increased Ta concentrations can be explained by the previously mentioned argument. It is caused by the effect of Ta that stabilizes the α phase in preference to the β phase; ie, the disappearance of α + β is a transformation from α + β to α. The softening of the unstable α and the gradual disappearance of β from the α + β regions is caused by the effect of Ta in which the SFE of the matrix is raised and the α phase is stabilized.

The role of the σ phase in the reduction of ductility is demonstrated in Figures 7 to 9. As the distance from the fractured

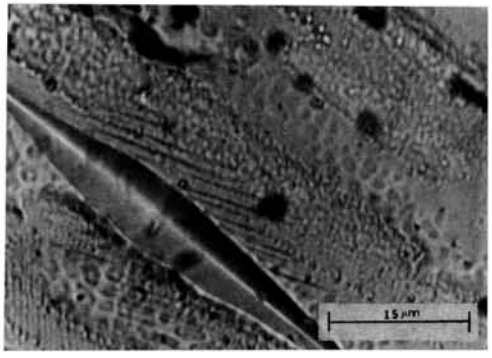

FIG 11.—Microstructure of alloy A_3B_3 (3.9% Ta) shows microhardness testing indentation and transformation ($\alpha \rightarrow \beta$) striations.

end decreased, the various regions of σ (KHN 772) were connected by minor cracks to surround a small region of the alloy. The σ phase is so hard that it physically prevents the continuity of the matrix. A σ-rich matrix is a matrix full of cracks. The application of the load causes the interconnections of these cracks which results in failure.

Conclusions

The experimental results of this study show that the addition of Ta to a 40 Co-30 Ni-30 Cr alloy has the following effects: There is formation of evenly distributed colonies of the Co-Cr-Ni-Ta phase. The phase was thought to be Co_3Ta because of its high hardness (KHN, 500 to 570). A decrease in the concentration of the less ductile matrix phase β and an increase in the ductile matrix phase α occurred. This was attributed to the effect of Ta in which the SFE of the alloy was raised. It contributed to the formation of the embrittling σ phase when the Ta concentration was less than 12.0%. If more than 12.0% Ta was added, large amounts of the σ phase formed. This effect may be caused by the effect of the higher concentrations of Ta on the average electron hole ($\bar{N}_v$) of the alloy and on the precipitation of σ.

References

1. MOHAMMED, H., and ASGAR, K.: A New Dental Superalloy System: I. Theory and Alloy Design, *J Dent Res* **52:**136-144, 1973.
2. MOHAMMED, H., and ASGAR, K.: A New Dental Superalloy System: II. Mechanical Properties, *J Dent Res* **52:**145-150, 1973.
3. COCHRAN, W.G., and COX, G.M.: *Experimental Design,* New York: Wiley and Sons, 1966.
4. FISHER, R.A.: *Statistical Methods for Research Workers,* 10th ed, London: Oliver and Boyd, 1946.
5. SIMS, C.T.: A Contemporary View of Cobalt-Base Alloys, *J Metals* **21:**27-42, 1969.
6. JOHNSON, R.S., JR.: Determinations of a Partial Room-Temperature Ternary Constitution Diagram in the As Cast Cr-Co-Ni System Utilizing a Factorial Experimental Design, PhD dissertation, University of Michigan, 1970.